
Denoising Fisher Training For Neural Implicit Samplers

Weijian Luo

Peking University
luoweijian@stu.pku.edu.cn
pkulwj1994@icloud.com

Wei Deng

Machine Learning Research,
Morgan Stanley, New York
weideng056@gmail.com

Abstract

Efficient sampling from un-normalized target distributions is pivotal in scientific computing and machine learning. While neural samplers have demonstrated potential with a special emphasis on sampling efficiency, existing neural implicit samplers still have issues such as poor mode covering behavior, unstable training dynamics, and sub-optimal performances. To tackle these issues, in this paper, we introduce Denoising Fisher Training (DFT), a novel training approach for neural implicit samplers with theoretical guarantees. We frame the training problem as an objective of minimizing the Fisher divergence by deriving a tractable yet equivalent loss function, which marks a unique theoretical contribution to assessing the intractable Fisher divergences. DFT is empirically validated across diverse sampling benchmarks, including two-dimensional synthetic distribution, Bayesian logistic regression, and high-dimensional energy-based models (EBMs). Notably, in experiments with high-dimensional EBMs, our best one-step DFT neural sampler achieves results on par with MCMC methods with up to 200 sampling steps, leading to a substantially greater efficiency over 100 times higher. This result not only demonstrates the superior performance of DFT in handling complex high-dimensional sampling but also sheds light on efficient sampling methodologies across broader applications.

1 INTRODUCTION

Efficiently drawing samples from un-normalized distributions is a fundamental issue in various domains of research, including Bayesian inference (Green, 1995), simulations in biology and physics (Schütte et al., 1999; Olsson, 1995), and the fields of generative modeling and machine learning (Xie et al., 2016; Andrieu et al., 2003). The goal is to generate sets of samples from a target distribution defined by a differentiable, but possibly not normalized, potential function, denoted as $\log q(\mathbf{x})$. The main challenge lies in ensuring the accuracy of the target distribution with minimal sampling costs, especially in simulations involving multi-modal distributions.

The sampling challenge can be tackled using two main methodologies. The first involves a range of Markov Chain Monte Carlo (MCMC) techniques (Hastings, 1970; Roberts and Rosenthal, 1998; Xifara et al., 2014; Neal, 2011). These techniques create Markov Chains that are designed to have the desired target distribution as their stationary distribution. By simulating these chains, random noises can be iteratively adjusted to stationary distributions following the target distribution. While MCMC methods are renowned for generating asymptotically unbiased samples, they often face computational inefficiencies, particularly when dealing with barriers in high-dimensional multi-modal distributions (Huang et al., 2024). This is largely due to the large number of iterations necessary to produce a batch of samples that accurately represent the target distribution.

The second category of methods is known as learning to sample (L2S) models (Levy et al., 2018; Hu et al., 2018; Wu et al., 2020; di Langosco et al., 2021; Arbel et al., 2021; Zhang and Chen, 2021; Matthews et al., 2022; Vargas et al., 2022; Lahlou et al., 2023). These models leverage modern neural networks for sampling, aiming to improve both the quality and efficiency of sample generation compared to traditional non-learning-based methods such as MCMCs.

arXiv:2411.01453v1 [cs.LG] 3 Nov 2024

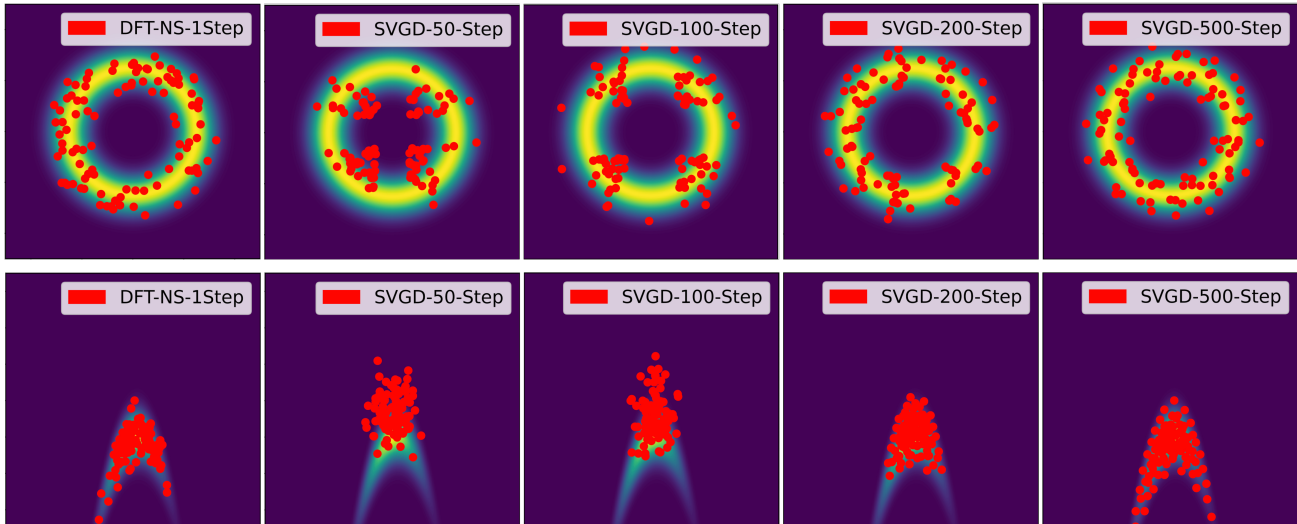


Figure 1: Visualizations of DFT neural sampler against Stein Variational Gradient Decent (Liu and Wang, 2016) with multiple sampling steps. The DFT-NS with 1 sampling step outperforms SVGD with 200 sampling steps. **Upper:** Donut target distribution in Table 1; **Under:** Rosenbrock target distribution in Table 1.

A prominent example within the L2S framework is the neural implicit sampler, which is recognized for its exceptional efficiency. An implicit neural sampler employs a transformation parametrized with a neural network to directly transform an easy-to-sample initial distribution to obtain final samples without multiple iterations. This can bypass the crucial challenge of sampling from multi-modal distributions via MCMCs and propose a direct transport from simple distributions to the target (Huang et al., 2024). As a result, the neural implicit sampler offers significant enhancements in efficiency and scalability using just one neural network pass. They are particularly beneficial in high-dimensional spaces, such as those encountered in image generations.

In this paper, we introduce Denoising Fisher Training (DFT), a novel approach for training neural implicit samplers to efficiently sample from un-normalized target distributions. We frame the training objective by minimizing the Fisher divergence between the implicit sampler and the target distribution. Though the direct objective is intractable, we introduce a tractable yet equivalent training objective in Section 4.1 with theoretical guarantees. Our theoretical assessments also introduce new tools for handling intractable Fisher divergences in broader applications. To evaluate the performance, efficiency, and scalability of DFT and the corresponding neural samplers, we have carried out empirical evaluations across three different sampling benchmarks with varying degrees of complexity in Section 5. The benchmarks include:

- Sampling from two-dimensional toy distributions;

- Bayesian inference with moderate dimensionality;
- Sampling from high-dimensional energy-based models (EBMs) using the MNIST dataset.

The experimental results consistently show that DFT samplers outperform existing methods in terms of sample quality. Notably, in the high-dimensional EBM tests, our neural samplers produced sample quality on par with the baseline EBM but with computational efficiency more than 200 times greater than traditional MCMC methods. These findings highlight the effectiveness, efficiency, and versatility of our proposed methods across a wide range of sampling scenarios.

2 RELATED WORKS

2.1 Neural Samplers

Neural networks have emerged as powerful tools in various domains, demonstrating their ability to produce diverse, high-quality samples. They have been successfully applied in tasks such as text-to-image generation (Brock et al., 2018; Karras et al., 2019, 2020, 2021; Nichol and Dhariwal, 2021; Dhariwal and Nichol, 2021; Ramesh et al.; Saharia et al., 2022; Rombach et al., 2022), audio generation (Huang et al., 2023), video and 3D creation (Clark et al., 2019; Ho et al., 2022a; Molad et al., 2023; Poole et al., 2022), and even molecule design (Nichol et al., 2021; Ho et al., 2022b). Recently, there has been a growing interest in leveraging neural networks for sampling from target distributions.

Three primary classes of neural networks have been

extensively studied for sampling tasks. The first class comprises normalizing flows (NFs) (Rezende and Mohamed, 2015), while the second class consists of diffusion models (DMs) (Song et al., 2021). NFs employ invertible neural transformations to map Gaussian latent vectors \mathbf{z} to obtain samples \mathbf{x} . The strict invertibility of NF transformations enables the availability of likelihood values for generated samples, which are differentiable with respect to the model’s parameters. Training NFs often involves minimizing the KL divergence between the NF and the target distribution (Wu et al., 2020). On the other hand, DMs employ neural score networks to model the marginal score functions of a data-initialized diffusion process. DMs have been successfully employed to enhance the sampler performance of the annealed importance sampling algorithm (Neal, 2001), a widely recognized MCMC method for various sampling benchmarks. Despite the successes of NFs and DMs, both models have their limitations. The invertibility of NFs restricts their expressiveness, which can hinder their ability to effectively model high-dimensional targets. Moreover, DMs still require a considerable number of iterations for sample generation, resulting in computational inefficiency.

2.2 Implicit Neural Samplers

Different from other neural samplers, neural implicit samplers are favored for their high efficiency and flexible modeling ability. Typically, an implicit generative model uses a flexible neural transform $g_\theta(\cdot)$ to push forward easy-to-sample noises $\mathbf{z} \sim p_z$ to obtain samples $\mathbf{x} = g_\theta(\mathbf{z})$. Though implicit samplers have multiple advantages, training them is not easy.

Research has explored various techniques for efficiently training neural implicit samplers by focusing on minimizing divergence. For example, the study by Hu et al. (2018) examines the training process through the reduction of the Stein discrepancy, while another study looks into practical algorithms designed to decrease the Kullback-Leibler divergence and the Fisher divergence. Although these approaches have shown promising results, they are not without their shortcomings. In particular, the methods intended to minimize Fisher divergence, despite their theoretical validity, have struggled to perform effectively with target distributions that exhibit high multi-modality (Luo et al., 2024). Besides, the training approach that minimizes the KL divergence also encounters sub-optimal performances (Luo et al., 2024). On the contrary, our introduced Denoising Fisher Training overcame the above issues by introducing a new stable and equivalent loss. Before we introduce the DFT, we give some background knowledge in Section 3.

3 BACKGROUND

Standard Score Matching. Score matching (Hyvärinen and Dayan, 2005) provided practical approaches to estimating score functions. Assume one only has available samples $\mathbf{x} \sim p$ and wants to use a parametric approximated distribution $q_\phi(\mathbf{x})$ to approximate p . Such an approximation can be made by minimizing the Fisher Divergence between p and q_ϕ with the definition

$$\mathcal{D}_{FD}(p, q_\phi) := \mathbb{E}_{\mathbf{x} \sim p} \left\{ \|\nabla_{\mathbf{x}} \log p(\mathbf{x})\|_2^2 + \|\nabla_{\mathbf{x}} \log q_\phi(\mathbf{x})\|_2^2 - 2\langle \nabla_{\mathbf{x}} \log p(\mathbf{x}), \nabla_{\mathbf{x}} \log q_\phi(\mathbf{x}) \rangle \right\}.$$

Under certain mild conditions, the objective equals to

$$\mathcal{L}(\phi) = \mathbb{E}_p \left\{ \|\nabla_{\mathbf{x}} \log q_\phi(\mathbf{x})\|_2^2 + 2\Delta_{\mathbf{x}} \log q_\phi(\mathbf{x}) \right\}. \quad (1)$$

This objective can be estimated only through samples from p , thus is tractable when q_ϕ is well-defined. Moreover, one only needs to define a score network $\mathbf{s}_\phi(\mathbf{x}): \mathbb{R}^D \rightarrow \mathbb{R}^D$ instead of a density model to represent the parametric score function. This technique was named after Score Matching. Other variants of score matching were also studied (Song et al., 2019; Pang et al., 2020; Meng et al., 2020; Lu et al., 2022; Bao et al., 2020).

Denoising Score Matching. Notice that the standard score-matching objective has a term $\Delta_{\mathbf{x}} \log q_\phi(\mathbf{x})$ that is computationally expensive. Denoising score matching (Vincent, 2011) is introduced to remedy this issue. The concept of denoising score matching is to perturb the sampling distribution by adding small Gaussian noises and then letting the score network match the conditional score functions. Specifically, let $\mathbf{x} \sim p$ be drawn from the sampling distribution. And let $\mathbf{x}_\sigma = \mathbf{x} + \sigma\epsilon$, $\epsilon \sim \mathcal{N}(\mathbf{0}, \mathcal{I})$. When σ is small, the distribution p_σ of \mathbf{x}_σ is a good approximation of the sampling distribution p of \mathbf{x}_0 . We use $p(\mathbf{x}_\sigma | \mathbf{x}_0)$ to denote the conditional distribution. If we want to use a parametric distribution q_ϕ (or a neural score function $\mathbf{s}_\phi(\cdot)$) to approximate the distribution of The matching objective of denoising score matching is to minimize

$$\mathcal{L}_{DSM}(\phi) = \mathbb{E}_{\substack{\mathbf{x}_0 \sim p, \\ \mathbf{x}_\sigma | \mathbf{x}_0 \sim p(\mathbf{x}_\sigma | \mathbf{x}_0)}} \left\{ \|\nabla_{\mathbf{x}_\sigma} \log q(\mathbf{x}_\sigma) - \nabla_{\mathbf{x}_\sigma} \log p(\mathbf{x}_\sigma | \mathbf{x}_0)\|_2^2 \right\}. \quad (2)$$

4 DENOISING FISHER TRAINING

In this section, we introduce the denoising Fisher training (DFT) method and show its equivalence to minimizing the Fisher divergence. The DFT incorporates

a noise-injection and denoising mechanism into the training of implicit sampler and shows significant stability than the previous Fisher training method in both theoretical and empirical aspects.

4.1 The Training Objective

The Problem Setup. Let $g_\theta(\cdot): \mathbb{R}^{D_z} \rightarrow \mathbb{R}^{D_x}$ be an implicit sampler (i.e., a neural network transform), p_z the latent distribution, p_θ the sampler induced distribution $\mathbf{x} = g_\theta(\mathbf{z})$, and $q(\mathbf{x})$ the un-normalized target. Our goal in this section is to train the implicit sampler g_θ such that $p_\theta(\mathbf{x})$ equals $q(\mathbf{x})$. Instead of directly minimizing the Fisher divergence between $p_\theta(\mathbf{x})$ and $q(\mathbf{x})$, we add some little noise to the implicit sampler to tweak the sampler distribution with

$$\mathbf{x}_\sigma := \mathbf{x}_0 + \sigma\epsilon, \quad \mathbf{x}_0 = g_\theta(\mathbf{z}), \quad \epsilon \sim \mathcal{N}(\mathbf{0}, \mathcal{I}) \quad (3)$$

Therefore the conditional distribution $p(\mathbf{x}_\sigma | \mathbf{x}_0) = \mathcal{N}(\mathbf{x}_0, \sigma^2 \mathcal{I})$ has an explicit form. When σ is set to be small, the distribution $p_{\theta, \sigma}$ which represents the distribution of \mathbf{x}_σ is a sufficiently good approximation of the implicit distribution p_θ of \mathbf{x}_0 . We denote $\mathbf{s}_q(\mathbf{x}_\sigma) := \nabla_{\mathbf{x}_\sigma} \log q(\mathbf{x}_\sigma)$ and $\mathbf{s}_{\theta, \sigma}(\mathbf{x}_\sigma) := \nabla_{\mathbf{x}_\sigma} \log p_{\theta, \sigma}(\mathbf{x}_\sigma)$. Our goal is to minimize the Fisher divergence between $p_{\sigma, \theta}(\mathbf{x})$ and $q(\mathbf{x})$ which writes

$$\mathcal{D}_{FD}(\theta) := \mathbb{E}_{\mathbf{x}_\sigma \sim p_{\theta, \sigma}} \|\mathbf{s}_q(\mathbf{x}_\sigma) - \mathbf{s}_{\theta, \sigma}(\mathbf{x}_\sigma)\|_2^2 \quad (4)$$

The Intractable Objective To make the derivation neat, we may use the notion $\mathbf{x}_\sigma(\theta)$ and \mathbf{x}_σ interchangeably to emphasize the parameter dependence of \mathbf{x}_σ and θ if necessary. In order to minimize the objective equation 4, we take the θ gradient for such an objective, which writes

$$\begin{aligned} \frac{\partial}{\partial \theta} \mathcal{D}_{FD}(\theta) &= \frac{\partial}{\partial \theta} \mathbb{E}_{\mathbf{x}_\sigma \sim p_{\theta, \sigma}} \|\mathbf{s}_q(\mathbf{x}_\sigma) - \mathbf{s}_{\theta, \sigma}(\mathbf{x}_\sigma)\|_2^2 \\ &= \mathbb{E}_{\mathbf{x}_\sigma \sim p_{\theta, \sigma}} \left\{ \frac{\partial}{\partial \mathbf{x}_\sigma} \left\{ \|\mathbf{s}_q(\mathbf{x}_\sigma) - \mathbf{s}_{\theta, \sigma}(\mathbf{x}_\sigma)\|_2^2 \right\} \frac{\partial \mathbf{x}_\sigma(\theta)}{\partial \theta} \right. \\ &\quad \left. - 2[\mathbf{s}_q(\mathbf{x}_\sigma) - \mathbf{s}_{\theta, \sigma}(\mathbf{x}_\sigma)]^T \frac{\partial}{\partial \theta} \mathbf{s}_{\theta, \sigma}(\mathbf{x}_\sigma) \right\} \\ &= \text{Grad}_1(\theta) + \text{Grad}_1(\theta). \end{aligned} \quad (5)$$

Where $\text{Grad}_1(\theta)$ and $\text{Grad}_2(\theta)$ are defined with

$$\begin{aligned} \text{Grad}_1(\theta) &= \mathbb{E}_{p_{\theta, \sigma}} \left\{ \frac{\partial}{\partial \mathbf{x}_\sigma} \left\{ \|\mathbf{s}_q(\mathbf{x}_\sigma) - \mathbf{s}_{\theta, \sigma}(\mathbf{x}_\sigma)\|_2^2 \right\} \frac{\partial \mathbf{x}_\sigma(\theta)}{\partial \theta} \right\}, \\ \text{Grad}_2(\theta) &= \mathbb{E}_{p_{\theta, \sigma}} \left\{ -2[\mathbf{s}_q(\mathbf{x}_\sigma) - \mathbf{s}_{\theta, \sigma}(\mathbf{x}_\sigma)]^T \frac{\partial}{\partial \theta} \mathbf{s}_{\theta, \sigma}(\mathbf{x}_\sigma) \right\}. \end{aligned}$$

The gradient formula of equation 5 considers all path derivatives concerning parameter θ . We put a detailed derivation in the Appendix.

Notice that the first gradient term $\text{Grad}_1(\theta)$ can be obtained if we stop the θ gradient for $\mathbf{s}_{\theta, \sigma}(\cdot)$, i.e. $\mathbf{s}_{\text{sg}[\theta], \sigma}(\cdot)$ and minimize a corresponding loss function

$$\begin{aligned} \mathcal{L}_1(\theta) &= \mathbb{E}_{\mathbf{x}_\sigma \sim p_{\theta, \sigma}} \left\{ \|\mathbf{s}_q(\mathbf{x}_\sigma) - \mathbf{s}_{\text{sg}[\theta], \sigma}(\mathbf{x}_\sigma)\|_2^2 \right\} \quad (6) \\ &= \mathbb{E}_{\substack{\mathbf{z} \sim p_z, \epsilon \sim \mathcal{N}(\mathbf{0}, \mathcal{I}) \\ \mathbf{x}_\sigma = g_\theta(\mathbf{z}) + \sigma\epsilon}} \left\{ \|\mathbf{s}_q(\mathbf{x}_\sigma) - \mathbf{s}_{\text{sg}[\theta], \sigma}(\mathbf{x}_\sigma)\|_2^2 \right\} \end{aligned}$$

However, the second gradient $\text{Grad}_2(\theta)$ include the term $\frac{\partial}{\partial \theta} \mathbf{s}_{\theta, \sigma}(\cdot)$ which is unknown yet intractable. This is because, for the implicit sampler, we only have efficient samples from the implicit distribution, but the score function $\mathbf{s}_{\theta, \sigma}(\cdot)$ along with its θ derivative is unknown.

The Tractable yet Equivalent Objective.

Though gradient $\text{Grad}_2(\theta)$ is intractable, fortunately, in this paper, we can address such an issue by introducing theoretical tools in Theorem 1.

Theorem 1. *If distribution $p_{\theta, \sigma}$ satisfies some wild regularity conditions, then we have for all vector-valued score function $\mathbf{s}_q(\cdot)$, the equation holds for all parameter θ :*

$$\begin{aligned} &\mathbb{E}_{\mathbf{x}_\sigma \sim p_{\theta, \sigma}} \left\{ -2[\mathbf{s}_q(\mathbf{x}_\sigma) - \mathbf{s}_{\theta, \sigma}(\mathbf{x}_\sigma)]^T \frac{\partial}{\partial \theta} \mathbf{s}_{\theta, \sigma}(\mathbf{x}_\sigma) \right\} \\ &= \frac{\partial}{\partial \theta} \mathbb{E}_{\substack{\mathbf{z} \sim p_z, \mathbf{x}_0 = g_\theta(\mathbf{z}), \\ \epsilon \sim \mathcal{N}(\mathbf{0}, \mathcal{I}), \mathbf{x}_\sigma = \mathbf{x}_0 + \sigma\epsilon}} \left\{ 2[\mathbf{s}_q(\mathbf{x}_\sigma) - \mathbf{s}_{\text{sg}[\theta], \sigma}(\mathbf{x}_\sigma)]^T \right. \\ &\quad \left. [\mathbf{s}_{\text{sg}[\theta], \sigma}(\mathbf{x}_\sigma) - \nabla_{\mathbf{x}_\sigma} \log p(\mathbf{x}_\sigma | \mathbf{x}_0)] \right\} \end{aligned} \quad (7)$$

We put the detailed proof in the Appendix. Theorem 1 shows that the intractable gradient $\text{Grad}_2(\theta)$ happens to be the same as the gradient of a tractable loss equation 7 if we can have a good pointwise approximation of the score network $\mathbf{s}_{\text{sg}[\theta], \sigma}(\cdot, \cdot)$. In practice, such an approximation is not difficult due to mature score function estimation techniques as we will discuss in Section 3. Therefore, we can minimize a tractable loss function equation 8 using gradient-based algorithms to get the intractable gradient $\text{Grad}_2(\theta)$:

$$\begin{aligned} \mathcal{L}_2(\theta) &= \mathbb{E}_{\substack{\mathbf{z} \sim p_z, \mathbf{x}_0 = g_\theta(\mathbf{z}), \\ \epsilon \sim \mathcal{N}(\mathbf{0}, \mathcal{I}), \mathbf{x}_\sigma = \mathbf{x}_0 + \sigma\epsilon}} \left\{ 2[\mathbf{s}_q(\mathbf{x}_\sigma) - \mathbf{s}_{\text{sg}[\theta], \sigma}(\mathbf{x}_\sigma)]^T \right. \\ &\quad \left. [\mathbf{s}_{\text{sg}[\theta], \sigma}(\mathbf{x}_\sigma) - \nabla_{\mathbf{x}_\sigma} \log p(\mathbf{x}_\sigma | \mathbf{x}_0)] \right\} \\ &= \mathbb{E}_{\substack{\mathbf{z} \sim p_z, \mathbf{x}_0 = g_\theta(\mathbf{z}), \\ \epsilon \sim \mathcal{N}(\mathbf{0}, \mathcal{I}), \mathbf{x}_\sigma = \mathbf{x}_0 + \sigma\epsilon}} \left\{ 2[\mathbf{s}_q(\mathbf{x}_\sigma) - \mathbf{s}_{\text{sg}[\theta], \sigma}(\mathbf{x}_\sigma)]^T \right. \\ &\quad \left. [\mathbf{s}_{\text{sg}[\theta], \sigma}(\mathbf{x}_\sigma) - \nabla_{\mathbf{x}_\sigma} \log p(\mathbf{x}_\sigma | \mathbf{x}_0)] \right\} \end{aligned} \quad (8)$$

Combining with equation 6 and equation 8 with equation 5, we can have the final equivalent loss function

that can minimize the Fisher divergence which writes

$$\mathcal{L}_{DFT}(\theta) = \mathcal{L}_1(\theta) + \mathcal{L}_2(\theta) \quad (9)$$

Where $\mathcal{L}_1(\theta)$ and $\mathcal{L}_2(\theta)$ are defined in equation 6 and equation 8. We name our training objective the denoising Fisher training objective because it originates from minimizing the Fisher divergence between the slightly tweaked sampler and the target distribution.

Algorithm 1: The Denoising Fisher Training (DFT) Algorithm for Neural Implicit Samplers.

Input: un-normalized target $\log q(\mathbf{x})$, latent distribution $p_z(\mathbf{z})$, implicit sampler $g_\theta(\cdot)$, score network $\mathbf{s}_\phi(\cdot)$, mini-batch size B , max iteration M .

Randomly initialize $(\theta^{(0)}, \phi^{(0)})$.

for t in $0:M$ **do**

// update score network parameter

 Freeze θ , free ϕ

 Get mini-batch without parameter dependence

$x_i = \text{sg}[g_{\theta^{(t)}}(\mathbf{z}_i)], \mathbf{z}_i \sim p_z(\mathbf{z}), i = 1, \dots, B$.

 Update Score network ϕ by minimizing equation 1 or equation 2, with samples drawn from implicit samplers and detach the θ gradient

// update sampler parameter

 Freeze ϕ , free θ

 Get mini-batch differentiable samples with θ -parameter-dependence

$\mathbf{x}_i = g_{\theta^{(t)}}(\mathbf{z}_i), \mathbf{z}_i \sim p_z(\mathbf{z}), i = 1, \dots, B$.

 Calculate loss with equation 9

 Update θ with gradient-based optimization algorithms to get $\theta^{(t+1)}$.

end

return (θ, ϕ) .

The Practical Algorithm Till now, we can formally define the denoising Fisher training algorithm for implicit samplers in the Algorithm 1. As we can see, the algorithm involves two neural networks, with one $g_\theta(\cdot)$ being the implicit sampler and $\mathbf{s}_\phi(\cdot)$ being the neural score network to estimate the score function of the implicit sampler. The algorithm involves iterations that alternatively update each neural network while freezing the other one. In the first step of each iteration, we freeze the θ and we generate a batch of samples efficiently from the neural implicit sampler g_θ . Then we use the generated samples to update the score network \mathbf{s}_ϕ to approximate the implicit sampler’s score function. In the second step, we freeze ϕ and minimize equation 9 to update g_θ .

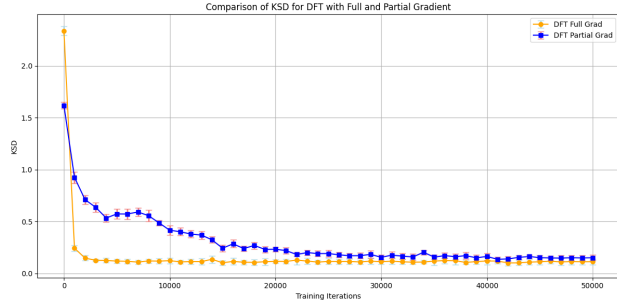


Figure 2: The comparison of KSD values of DFT-NS using full and partial gradients in equation 5.

5 EXPERIMENTS

In this section, we validate neural samplers trained with DFT across a range of three distinct sampling benchmarks following Luo et al. (2024). These benchmarks span a spectrum of complexity, from low-dimensional (2-dimensional targets) to high-dimensional (784-dimensional image targets) tasks.

5.1 2D Synthetic Target Sampling

Experiment Settings. We leverage the open-source implementation from Sharrock and Nemeth (2023)¹ and adhere to the experimental configurations established by Luo et al. (2024) for the training of samplers on six 2D target distributions. Our comparison encompasses a range of methods, including 3 MCMC baselines: Stein variational gradient descent (SVGD) (Liu and Wang, 2016), Langevin dynamics (LD) (Welling and Teh, 2011), and Hamiltonian Monte Carlo (HMC) (Neal et al., 2011); one explicit baseline: coupling normalizing flow (Dinh et al., 2016); and four implicit samplers: KL training sampler (Luo et al., 2024), Fisher training sampler (Luo et al., 2024), KSD neural sampler (KSD-NS) (Hu et al., 2018), and SteinGan (Wang and Liu, 2016). All implicit samplers are designed with a uniform neural architecture, which consists of a four-layer multilayer perceptron (MLP) with 400 hidden units per layer, and employ ELU activation functions for both the sampler and the score network where applicable.

We evaluate sampling results with kernelized Stein’s discrepancy (KSD) (Liu et al., 2016), which is a widely used metric for evaluating the quality of a batch of samples to a target distribution with score functions (Liu et al., 2016; Gorham and Mackey, 2015). In our evaluations, we utilize the KSD with the inverse multiquadric (IMQ) kernel, which is implemented through

¹<https://github.com/louissharrock/coin-svgd>

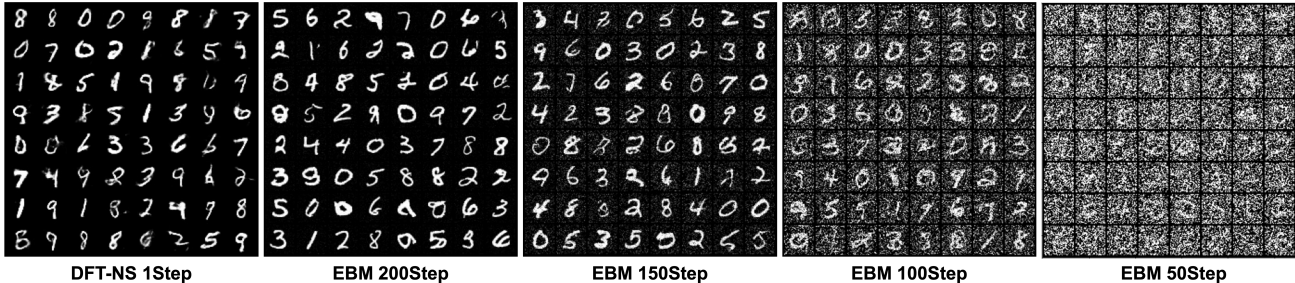


Figure 3: A visualization of DFT-NS on MNIST against default MCMC sampling result from DeepEBM. The one-step DFT-NS outperforms MCMC samplers with 200 sampling steps as shown in Table 3.

the open-source package `sgmcmcjax`². We put the quantitative results in Table 1.

Across all target distributions, we have trained all implicit neural samplers (DFT-NS in Table 1) using the Adam optimizer. We use the learning rate of $2e-5$ and a batch size of 5000 by default unless specifically claimed. To evaluate the kernelized Stein’s discrepancy (KSD), we have conducted assessments every 1000 iterations, using 500 samples and repeating the process 20 times for each evaluation. The lowest mean KSD observed during training iterations has been selected as our final result. The neural architecture and evaluation setup is the same as Luo et al. (2024).

Performance Analysis. As Table 1 shows, The Stein variational gradient descent (SVGD) with 500 sampling steps shows the best KSD values. However, when the sampling steps of SVGD are limited to less than 200, the performance drops significantly. For relatively simple target distribution such as Gaussian distribution, the SteinGAN is the best. However, for complex targets such as Donut, Funnel, and Squiggle distributions, the DFT-NS is the best among all neural samplers. The visualization in Figure 1 qualitatively confirms the quantitative observation.

Notice in equation 5, we decompose the gradient into two terms. In Figure 2, we compare the samplers’ KSD that is trained using full gradient equation 5 and solely the second gradient $\text{Grad}_2(\theta)$ which we term the DFT partial grad on Funnel distribution. The results show that using a full gradient is consistently better than the partial gradient. However, as we can see, only using $\text{Grad}_2(\theta)$ still leads to solid training. In our practical experiments, we find that sometimes balancing both gradients can result in better performances than using both or one of them.

In summary, across both analytic and neural targets, DFT-NS demonstrate a marked advantage in efficiency while maintaining comparable or better performance

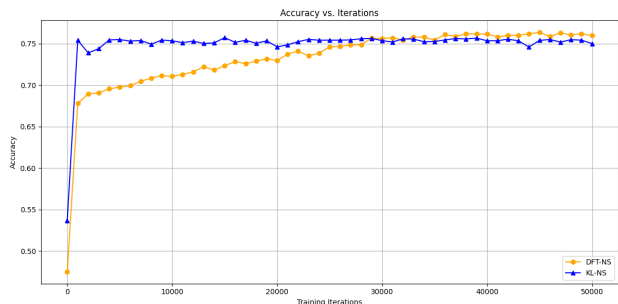


Figure 4: The test-accuracy curve of DFT-NS (ours) and KL-NS (Luo et al., 2024) for Bayesian Logistic Regression. Though KL-NS converges faster, DFT-NS shows better final accuracy than KL-NS with sufficient training iterations.

than MCMC samplers. This efficiency makes DFT-NS a more viable option for a wide array of sampling tasks where high efficiency and reduced computational costs are of the essence.

5.2 Bayesian Logistic Regression

Having established the effectiveness of our sampler on low-dimensional 2D target distributions in the previous section, we now turn our attention to more complex, real-world scenarios. Bayesian logistic regression offers a set of medium-dimensional target distributions (ranging from 10 to 100 dimensions) that are ideal for this purpose. In this section, we pit our DFT neural samplers on solving this problem following Hu et al. (2018) and Luo et al. (2024).

The primary objective of this experiment is to assess the performance of our proposed sampler in terms of test accuracy when applied to Bayesian logistic regression tasks. To provide a comprehensive evaluation, we also compare our sampler’s performance against that of various MCMC samplers. This comparison will shed light on how our sampler stacks up against existing methods in a real-world application, allowing us to

²<https://github.com/jeremiecoullon/SGMCMCJax>

Table 1: KSD values of samplers. For MCMC, we set the Stepsize=0.01, num particles=500, num chains=20.

Sampler	Gaussian	MOG2	Rosenbrock	Donut	Funnel	Squiggle
MCMC						
SVGD(500)	0.013 ± 0.001	0.044 ± 0.006	0.053 ± 0.002	0.057 ± 0.004	0.052 ± 0.001	0.024 ± 0.002
SVGD(200)	0.0367 ± 0.016	0.0545 ± 0.006	0.513 ± 0.040	0.0834 ± 0.007	0.0502 ± 0.002	0.0391 ± 0.006
SVGD(100)	0.776 ± 0.069	0.688 ± 0.027	1.498 ± 0.078	0.361 ± 0.023	0.189 ± 0.023	0.156 ± 0.017
SVGD (50)	1.681 ± 0.073	1.170 ± 0.030	2.673 ± 0.163	1.089 ± 0.035	0.612 ± 0.072	0.682 ± 0.045
LD(500)	0.107 ± 0.025	0.099 ± 0.008	0.152 ± 0.030	0.107 ± 0.020	0.116 ± 0.029	0.139 ± 0.030
LD(200)	0.141 ± 0.024	0.109 ± 0.020	0.284 ± 0.037	0.109 ± 0.021	0.144 ± 0.017	0.176 ± 0.057
LD(100)	0.277 ± 0.042	0.276 ± 0.018	0.691 ± 0.030	0.115 ± 0.024	0.231 ± 0.029	0.264 ± 0.055
LD (50)	0.669 ± 0.073	0.678 ± 0.016	1.198 ± 0.038	0.246 ± 0.037	0.387 ± 0.033	0.419 ± 0.046
HMC(500)	0.094 ± 0.020	0.106 ± 0.020	0.134 ± 0.034	0.113 ± 0.020	0.135 ± 0.010	0.135 ± 0.033
HMC(200)	0.109 ± 0.025	0.104 ± 0.018	0.137 ± 0.023	0.107 ± 0.016	0.132 ± 0.028	0.143 ± 0.024
HMC(100)	0.114 ± 0.031	0.106 ± 0.018	0.205 ± 0.031	0.115 ± 0.017	0.129 ± 0.029	0.159 ± 0.038
HMC (50)	0.199 ± 0.038	0.176 ± 0.033	0.501 ± 0.032	0.112 ± 0.019	0.176 ± 0.033	0.234 ± 0.046
NEURAL SAMPLERS						
COUP-FLOW	0.102 ± 0.028	0.158 ± 0.019	0.150 ± 0.026	0.239 ± 0.013	0.269 ± 0.019	0.130 ± 0.026
KSD-NS	0.206 ± 0.043	1.129 ± 0.197	1.531 ± 0.058	0.341 ± 0.039	0.396 ± 0.221	0.462 ± 0.065
STEINGAN	0.091 ± 0.013	0.131 ± 0.011	0.121 ± 0.022	0.104 ± 0.013	0.129 ± 0.020	0.124 ± 0.018
FISHER-NS	0.095 ± 0.016	0.118 ± 0.013	0.157 ± 0.030	0.179 ± 0.028	7.837 ± 1.614	0.202 ± 0.037
KL-NS	0.099 ± 0.015	0.104 ± 0.015	0.123 ± 0.021	0.109 ± 0.015	0.115 ± 0.012	0.118 ± 0.024
DFT-NS	0.098 ± 0.019	0.101 ± 0.025	0.121 ± 0.016	0.100 ± 0.013	0.081 ± 0.009	0.115 ± 0.018

evaluate its practical utility and effectiveness in handling medium-dimensional target distributions.

Experiment settings. We have adopted the experimental setup similar to that of [Hu et al. \(2018\)](#) for the Bayesian logistic regression tasks. The Covertype dataset, which comprises 54 features and 581,012 observations, is a well-established benchmark for Bayesian inference. In line with [Hu et al. \(2018\)](#), we have specified the prior distribution for the weights as $p(w|\alpha) = \mathcal{N}(w; 0, \alpha^{-1})$ and for α as $p(\alpha) = \text{Gamma}(\alpha; 1, 0.01)$. The dataset has been randomly divided into a training set, accounting for 80

Our objective is to develop an implicit DFT neural sampler that can efficiently sample from the posterior distribution. Once trained, the implicit sampler not only delivers the best accuracy but also operates hundreds of times faster than MCMC methods. In this experiment, we train DFT-NS and KL-NS using the same configuration as proposed in [Luo et al. \(2024\)](#). Our evaluation metric is the test accuracy, which marks how well samplers can solve the Bayesian logistic regression.

Performance Analysis. Table 2 shows the quantitative performances of different samplers. As we can see, the DFT with full loss in equation 9 results in the best test accuracy of 76.36%, outperforming KL-NS [Luo et al. \(2024\)](#), Fisher-NS ([Hu et al., 2018](#)), and MCMC algorithms. The DFT-NS with only the second loss of equation 8 also shows a decent performance.

We also conduct a detailed comparison of DFT-NS with KL-NS in Figure 4 by recording the test accuracy of both samplers along the training process. The

results show that KL-NS converges faster than DFT-NS, however, DFT-NS archives a better final test accuracy with sufficient training iterations. These experiments underscore the capability of our proposed training method to effectively manage real-world Bayesian inference tasks involving medium-dimensional data.

Table 2: Test Accuracies for Bayesian Logistic Regression on Covertype Dataset following [Hu et al. \(2018\)](#). DFT-NS is the neural implicit sampler trained with DFT with full loss in equation 9. DFT-NS* means we only use the second loss equation 8 for training.

SGLD	DSVI
75.09% ± 0.20%	73.46% ± 4.52%
SVGD	STEINGAN
74.76% ± 0.47%	75.37% ± 0.19%
FISHER-NS	KL-IS(OURS)
76.22% ± 0.43%	75.95% ± 0.002%
DFT-NS(Ours)*	DFT-NS(Ours)
75.79% ± 0.55%	76.36% ± 0.009%

5.3 Sampling from Energy-based Models

A pivotal benefit of employing an implicit sampler is its superior inference efficiency, which is particularly advantageous for applications where traditional sampling methods fall short, such as in the context of high-dimensional energy-based models (EBMs). The inefficiency of default sampling methods in these scenarios often stems from the complex and intricate nature of the models, which can make sampling a computationally demanding task.

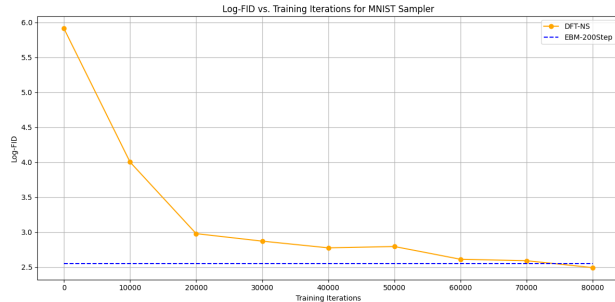


Figure 5: The Log-FID curve of one-step DFT-NS on MNIST image distribution. The blue dashed line marks the logarithm of FID of 200-step MCMC (Annealed Langevin dynamics) samples from pre-trained DeepEBM (Li et al., 2019).

Table 3: Comparison of Sampling Efficiency and FID values of multi-step MCMC samplers and one-step DFT neural sampler. The larger the FLOPS is, the more costs the sampler has.

Model	Steps	Infer Time (Sec)	FLOPS	FID
EBM	250	0.8455	0.58G × 250	9.54
EBM	200	0.6658	0.58G × 200	12.76
EBM	150	0.5115	0.58G × 150	165.07
EBM	100	0.3455	0.58G × 100	423.95
EBM	50	0.1692	0.58G × 50	519.04
DFT-NS	1	0.0012	1.11G	12.07

Experiment settings. A neural network in an energy-based model (EBM) (LeCun et al., 2006) defines a negative energy function, essentially the log of an un-normalized probability distribution. Post-training, extracting samples from an EBM typically involves an annealed Markov Chain Monte Carlo process (Xie et al., 2016), which is quite computationally demanding. In this experiment, we follow Luo et al. (2024) to evaluate the performance of DFT-NS to learn to sample from a deep EBM (Li et al., 2019) pre-trained on the MNIST image dataset. Considering the characteristics of image data, we closely follow Luo et al. (2024) to construct the neural sampler by stacking multiple convolutional neural network blocks. It processes a random Gaussian input of 128 dimensions to produce a 32x32 tensor, matching the resolution of the EBM’s training. We pre-train the DeepEBM in-house following Li et al. (2019). Then we train the CNN-based implicit neural sampler with DFT using the un-normalized probability induced by the pre-trained DeepEBM. We follow the training settings of Luo et al. (2024), using a batch size of 128 and Adam optimizer with a learning rate of 1e-4 on a single Nvidia-A100 GPU. The hours for one training trial is roughly three hours, which is conceptually cheap.

To quantitatively evaluate DFT-NS and MCMC samplers, we follow Luo et al. (2024); Heusel et al. (2017)

to train an MNIST classifier and compute the Fréchet Inception Distance (FID) (Heusel et al., 2017) using features extracted from the pre-trained classifier. We constructed the classifier with the wide-resnet neural network (Zagoruyko and Komodakis, 2016). We compare the FID of samples generated from one-step DFT-NS and multi-step MCMCs with the DeepEBM. The smaller the FID is, the better the sample quality is.

Performance. Table 3 shows the FID values and corresponding computational costs of each sampler. DFT-NS produces samples with better FID values than MCMC samplers with 200 sampling steps. But it is worse than MCMC samples with 250 sampling steps. This indicates that DFT-NS is better than MCMC with an acceleration rate larger than 200. Figure 3 shows a visualization of samples drawn from DFT-NS and MCMC samplers. This visualization qualitatively confirms the quantitative results in Table 3.

In Figure 3, we visualize the FID curve of the one-step DFT-NS versus the training iterations. We can conclude that DFT is a solid training approach that trains the neural implicit samplers to have a steady performance curve with the increase of training iterations.

6 CONCLUSION AND LIMITATIONS

In this paper, we’ve introduced denoising implicit training (DFT), an innovative technique for training implicit samplers to draw samples from distributions with un-normalized density. We’ve shown theoretically that DFT is equivalent to minimizing the Fisher divergence between a slightly tweaked neural sampler distribution and the target distribution. Through intensive quantitative experiments on scales of small, medium, and high dimensions, we show that neural samplers trained with DFT have better performances than other neural samplers and MCMC samplers with a decent number of sampling steps. Besides, our theoretical assessments on deriving the tractable loss may shed light on broader applications when handling intractable Fisher divergences.

Nevertheless, there are certain limitations to our proposed methods. First, the process of score estimation is not computationally inexpensive, making it a crucial avenue for research to develop a more efficient training algorithm that could eliminate the score estimation phase. Furthermore, currently, our sampler is confined to sampling tasks. Exploring how to extend this methodology to other applications, such as generative modeling, presents another intriguing area for future investigation.

References

- P. J. Green, “Reversible jump markov chain monte carlo computation and bayesian model determination,” *Biometrika*, vol. 82, no. 4, pp. 711–732, 1995.
- C. Schütte, A. Fischer, W. Huisinga, and P. Deuffhard, “A direct approach to conformational dynamics based on hybrid monte carlo,” *Journal of Computational Physics*, vol. 151, no. 1, pp. 146–168, 1999.
- P. Olsson, “Two phase transitions in the fully frustrated xy model,” *Physical review letters*, vol. 75, no. 14, p. 2758, 1995.
- J. Xie, Y. Lu, S.-C. Zhu, and Y. Wu, “A theory of generative convnet,” in *International Conference on Machine Learning*. PMLR, 2016, pp. 2635–2644.
- C. Andrieu, N. De Freitas, A. Doucet, and M. I. Jordan, “An introduction to mcmc for machine learning,” *Machine learning*, vol. 50, no. 1, pp. 5–43, 2003.
- Q. Liu and D. Wang, “Stein variational gradient descent: A general purpose bayesian inference algorithm,” *Advances in neural information processing systems*, vol. 29, 2016.
- W. Hastings, “Monte carlo sampling methods using markov chains and their applications,” *Biometrika*, vol. 57, no. 1, pp. 97–109, 1970.
- G. O. Roberts and J. S. Rosenthal, “Optimal scaling of discrete approximations to langevin diffusions,” *Journal of the Royal Statistical Society: Series B (Statistical Methodology)*, vol. 60, no. 1, pp. 255–268, 1998.
- T. Xifara, C. Sherlock, S. Livingstone, S. Byrne, and M. Girolami, “Langevin diffusions and the metropolis-adjusted langevin algorithm,” *Statistics & Probability Letters*, vol. 91, pp. 14–19, 2014.
- R. M. Neal, “Mcmc using hamiltonian dynamics,” in *Handbook of Markov Chain Monte Carlo*. Chapman and Hall/CRC, 2011, pp. 139–188.
- X. Huang, H. Dong, Y. Hao, Y. Ma, and T. Zhang, “Reverse diffusion monte carlo,” in *International Conference on Learning Representations (ICLR)*, 2024.
- D. Levy, M. D. Hoffman, and J. Sohl-Dickstein, “Generalizing hamiltonian monte carlo with neural networks,” in *International Conference on Learning Representations*, 2018.
- T. Hu, Z. Chen, H. Sun, J. Bai, M. Ye, and G. Cheng, “Stein neural sampler,” *arXiv preprint arXiv:1810.03545*, 2018.
- H. Wu, J. Köhler, and F. Noé, “Stochastic normalizing flows,” *Advances in Neural Information Processing Systems*, vol. 33, pp. 5933–5944, 2020.
- L. L. di Langosco, V. Fortuin, and H. Strathmann, “Neural variational gradient descent,” *arXiv preprint arXiv:2107.10731*, 2021.
- M. Arbel, A. Matthews, and A. Doucet, “Annealed flow transport monte carlo,” in *International Conference on Machine Learning*. PMLR, 2021, pp. 318–330.
- Q. Zhang and Y. Chen, “Path integral sampler: A stochastic control approach for sampling,” in *International Conference on Learning Representations*, 2021.
- A. Matthews, M. Arbel, D. J. Rezende, and A. Doucet, “Continual repeated annealed flow transport monte carlo,” in *International Conference on Machine Learning*. PMLR, 2022, pp. 15 196–15 219.
- F. Vargas, W. S. Grathwohl, and A. Doucet, “Denoising diffusion samplers,” in *The Eleventh International Conference on Learning Representations*, 2022.
- S. Lahlou, T. Deleu, P. Lemos, D. Zhang, A. Volokhova, A. Hernández-García, L. N. Ezzine, Y. Bengio, and N. Malkin, “A theory of continuous generative flow networks,” in *International Conference on Machine Learning*. PMLR, 2023, pp. 18 269–18 300.
- A. Brock, J. Donahue, and K. Simonyan, “Large scale gan training for high fidelity natural image synthesis,” in *International Conference on Learning Representations*, 2018.
- T. Karras, S. Laine, and T. Aila, “A style-based generator architecture for generative adversarial networks,” in *Proceedings of the IEEE/CVF conference on computer vision and pattern recognition*, 2019, pp. 4401–4410.
- T. Karras, S. Laine, M. Aittala, J. Hellsten, J. Lehtinen, and T. Aila, “Analyzing and improving the image quality of stylegan,” in *Proceedings of the IEEE/CVF conference on computer vision and pattern recognition*, 2020, pp. 8110–8119.
- T. Karras, M. Aittala, S. Laine, E. Härkönen, J. Hellsten, J. Lehtinen, and T. Aila, “Alias-free generative adversarial networks,” *Advances in Neural Information Processing Systems*, vol. 34, pp. 852–863, 2021.
- A. Q. Nichol and P. Dhariwal, “Improved denoising diffusion probabilistic models,” in *International Conference on Machine Learning*. PMLR, 2021, pp. 8162–8171.
- P. Dhariwal and A. Nichol, “Diffusion models beat gans on image synthesis,” *Advances in neural information processing systems*, vol. 34, pp. 8780–8794, 2021.

- A. Ramesh, P. Dhariwal, A. Nichol, C. Chu, and M. Chen, "Hierarchical text-conditional image generation with clip latents."
- C. Saharia, W. Chan, S. Saxena, L. Li, J. Whang, E. L. Denton, K. Ghasemipour, R. Gontijo Lopes, B. Karagol Ayan, T. Salimans *et al.*, "Photorealistic text-to-image diffusion models with deep language understanding," *Advances in Neural Information Processing Systems*, vol. 35, pp. 36 479–36 494, 2022.
- R. Rombach, A. Blattmann, D. Lorenz, P. Esser, and B. Ommer, "High-resolution image synthesis with latent diffusion models," in *Proceedings of the IEEE/CVF conference on computer vision and pattern recognition*, 2022, pp. 10 684–10 695.
- R. Huang, J. Huang, D. Yang, Y. Ren, L. Liu, M. Li, Z. Ye, J. Liu, X. Yin, and Z. Zhao, "Make-an-audio: Text-to-audio generation with prompt-enhanced diffusion models," *arXiv preprint arXiv:2301.12661*, 2023.
- A. Clark, J. Donahue, and K. Simonyan, "Adversarial video generation on complex datasets," *arXiv preprint arXiv:1907.06571*, 2019.
- J. Ho, W. Chan, C. Saharia, J. Whang, R. Gao, A. Gritsenko, D. P. Kingma, B. Poole, M. Norouzi, D. J. Fleet *et al.*, "Imagen video: High definition video generation with diffusion models," *arXiv preprint arXiv:2210.02303*, 2022.
- E. Molad, E. Horwitz, D. Valevski, A. R. Acha, Y. Matias, Y. Pritch, Y. Leviathan, and Y. Hoshen, "Dreamix: Video diffusion models are general video editors," *arXiv preprint arXiv:2302.01329*, 2023.
- B. Poole, A. Jain, J. T. Barron, and B. Mildenhall, "Dreamfusion: Text-to-3d using 2d diffusion," in *The Eleventh International Conference on Learning Representations*, 2022.
- A. Nichol, P. Dhariwal, A. Ramesh, P. Shyam, P. Mishkin, B. McGrew, I. Sutskever, and M. Chen, "Glide: Towards photorealistic image generation and editing with text-guided diffusion models," in *International Conference on Machine Learning*, 2021.
- J. Ho, T. Salimans, A. Gritsenko, W. Chan, M. Norouzi, and D. J. Fleet, "Video diffusion models," *arXiv preprint arXiv:2204.03458*, 2022.
- D. Rezende and S. Mohamed, "Variational inference with normalizing flows," in *International conference on machine learning*. PMLR, 2015, pp. 1530–1538.
- Y. Song, J. Sohl-Dickstein, D. P. Kingma, A. Kumar, S. Ermon, and B. Poole, "Score-based generative modeling through stochastic differential equations," in *International Conference on Learning Representations*, 2021.
- R. M. Neal, "Annealed importance sampling," *Statistics and computing*, vol. 11, no. 2, pp. 125–139, 2001.
- W. Luo, B. Zhang, and Z. Zhang, "Entropy-based training methods for scalable neural implicit samplers," *Advances in Neural Information Processing Systems*, vol. 36, 2024.
- A. Hyvärinen and P. Dayan, "Estimation of non-normalized statistical models by score matching." *Journal of Machine Learning Research*, vol. 6, no. 4, 2005.
- Y. Song, S. Garg, J. Shi, and S. Ermon, "Sliced score matching: A scalable approach to density and score estimation," in *Proceedings of the Thirty-Fifth Conference on Uncertainty in Artificial Intelligence, UAI 2019, Tel Aviv, Israel, July 22-25, 2019*, 2019, p. 204.
- T. Pang, K. Xu, C. Li, Y. Song, S. Ermon, and J. Zhu, "Efficient learning of generative models via finite-difference score matching," *Advances in Neural Information Processing Systems*, vol. 33, pp. 19 175–19 188, 2020.
- C. Meng, L. Yu, Y. Song, J. Song, and S. Ermon, "Autoregressive score matching," *Advances in Neural Information Processing Systems*, vol. 33, pp. 6673–6683, 2020.
- C. Lu, K. Zheng, F. Bao, J. Chen, C. Li, and J. Zhu, "Maximum likelihood training for score-based diffusion odes by high order denoising score matching," in *International Conference on Machine Learning*. PMLR, 2022, pp. 14 429–14 460.
- F. Bao, C. Li, K. Xu, H. Su, J. Zhu, and B. Zhang, "Bi-level score matching for learning energy-based latent variable models," *Advances in Neural Information Processing Systems*, vol. 33, pp. 18 110–18 122, 2020.
- P. Vincent, "A connection between score matching and denoising autoencoders," *Neural computation*, vol. 23, no. 7, pp. 1661–1674, 2011.
- L. Sharrock and C. Nemeth, "Coin sampling: Gradient-based bayesian inference without learning rates," *arXiv preprint arXiv:2301.11294*, 2023.
- M. Welling and Y. W. Teh, "Bayesian learning via stochastic gradient langevin dynamics," in *Proceedings of the 28th international conference on machine learning (ICML-11)*, 2011, pp. 681–688.
- R. M. Neal *et al.*, "Mcmc using hamiltonian dynamics," *Handbook of markov chain monte carlo*, vol. 2, no. 11, p. 2, 2011.
- L. Dinh, J. N. Sohl-Dickstein, and S. Bengio, "Density estimation using real nvp," *ArXiv*, vol. abs/1605.08803, 2016.

- D. Wang and Q. Liu, “Learning to draw samples: With application to amortized mle for generative adversarial learning,” *arXiv preprint arXiv:1611.01722*, 2016.
- Q. Liu, J. Lee, and M. I. Jordan, “A kernelized stein discrepancy for goodness-of-fit tests,” in *International Conference on Machine Learning*, 2016.
- J. Gorham and L. Mackey, “Measuring sample quality with stein’s method,” *Advances in Neural Information Processing Systems*, vol. 28, 2015.
- Z. Li, Y. Chen, and F. T. Sommer, “Learning energy-based models in high-dimensional spaces with multi-scale denoising score matching,” *arXiv preprint arXiv:1910.07762*, 2019.
- Y. LeCun, S. Chopra, R. Hadsell, A. Ranzato, and F. J. Huang, “A tutorial on energy-based learning,” 2006.
- M. Heusel, H. Ramsauer, T. Unterthiner, B. Nessler, and S. Hochreiter, “GANs trained by a two time-scale update rule converge to a local Nash equilibrium,” in *Advances in Neural Information Processing Systems*, 2017, pp. 6626–6637.
- S. Zagoruyko and N. Komodakis, “Wide residual networks,” *arXiv preprint arXiv:1605.07146*, 2016.
- M. Zhou, H. Zheng, Z. Wang, M. Yin, and H. Huang, “Score identity distillation: Exponentially fast distillation of pretrained diffusion models for one-step generation,” in *International Conference on Machine Learning*, 2024. [Online]. Available: <https://arxiv.org/abs/2404.04057>
- J. A. Blackard and D. J. Dean, “Comparative accuracies of artificial neural networks and discriminant analysis in predicting forest cover types from cartographic variables,” *Computers and Electronics in Agriculture*, vol. 24, pp. 131–151, 1999.
- M. K. Titsias and M. Lázaro-Gredilla, “Doubly stochastic variational bayes for non-conjugate inference,” in *International Conference on Machine Learning*, 2014.
- D. Hendrycks and K. Gimpel, “Gaussian error linear units (gelus),” *arXiv: Learning*, 2016.
- K. He, X. Zhang, S. Ren, and J. Sun, “Deep residual learning for image recognition,” *2016 IEEE Conference on Computer Vision and Pattern Recognition (CVPR)*, pp. 770–778, 2015.

A Pseudo Code for DFT Algorithm for Training Samplers from EBM

Algorithm 2: Pytorch Style Pseudo Python Code for the DFT Training Method

input : Generator G , Discriminator D , Diffusion process $diffusion$, Energy function $energy_fun$,
Maximum iterations max_iter , Batch size $batch_size$, Optimizer arguments for D and G ,
Annealing flag $anneal$, Validation interval $val_interval$, Number of discriminator steps D_steps ,
Distillation method $distill_method$, Prefix $prefix$

output: Trained generator G and discriminator D

$device \leftarrow 'cuda'$

$D_{optim} \leftarrow Adam(D.parameters(), **D_opt_args)$

$G_{optim} \leftarrow Adam(G.parameters(), **G_opt_args)$

for $iiter \in \{0, 1, \dots, max_iter\}$ **do**

if $distill_method == 'dft - full'$ **then**

$D.train().requires_grad_(\text{True})$

$G.eval().requires_grad_(\text{False})$

for $_ \in \{1, 2, \dots, D_steps\}$ **do**

$z \leftarrow torch.randn((batch_size, G.latent_dim, 1, 1)).cuda()$

$fake_x \leftarrow G(z)$

$t \leftarrow \text{random choice from } \{1, 2, \dots, diffusion.T\}$

$fake_t, t, noise, sigma_t, g2_t \leftarrow diffusion(fake_x, t = t, return_t = \text{True})$

$wgt \leftarrow g2_t / sigma_t.square()$

$d_loss \leftarrow 0.5 \times wgt \times (D(fake_t, t) + noise).square().sum([1, 2, 3])$

$d_loss \leftarrow d_loss.mean()$

$D_{optim}.zero_grad()$

$d_loss.backward()$

$D_{optim}.step()$

end

 Append $d_loss.item()$ to $dlosses$

$D.eval().requires_grad_(\text{False})$

$G.train().requires_grad_(\text{True})$

$z \leftarrow torch.randn((batch_size, G.latent_dim, 1, 1)).to(device)$

$fake_x \leftarrow G(z)$

$t \leftarrow \text{random choice from } \{7, 8, \dots, 50\}$

$fake_t, t, noise, sigma_t, g2_t \leftarrow diffusion(fake_x, t = t, return_t = \text{True})$

$sigma_t \leftarrow sigma_t.view(-1, 1, 1, 1)$

$fake_t \leftarrow fake_t.clone().detach().requires_grad_(\text{True})$

$lam \leftarrow 1.0$

$score_true \leftarrow torch.autograd.grad(energy_fun(fake_t, lam = lam).sum(), fake_t, create_graph = \text{True}, retain_graph = \text{True})[0] / sigma_t$

$score_fake \leftarrow D(fake_t, t) / sigma_t$

$score_diff \leftarrow score_fake - score_true$

$cond_score \leftarrow -noise / sigma_t$

$dloss_dx \leftarrow -2 \times (score_diff \times (score_fake - cond_score)).sum([1, 2, 3])$

$dloss_dx \leftarrow sigma_t * * 2 \times torch.autograd.grad(dloss_dx.sum(), fake_t, create_graph = \text{False}, retain_graph = \text{False})[0]$

$g_loss \leftarrow g2_t \times (dloss_dx \times fake_t).sum([1, 2, 3])$

$g_loss \leftarrow g_loss.mean()$

$G_{optim}.zero_grad()$

$g_loss.backward()$

$G_{optim}.step()$

 Append $g_loss.item()$ to $glosses$

end

if $iiter \bmod val_interval == 0$ **then**

 Save and plot intermediate results

end

end

B Theory

B.1 Proof of equation 5

Proof.

$$\begin{aligned} \frac{\partial}{\partial \theta} \mathcal{D}_{FD}(\theta) &= \frac{\partial}{\partial \theta} \mathbb{E}_{\mathbf{x}_\sigma \sim p_{\theta, \sigma}} \|\mathbf{s}_q(\mathbf{x}_\sigma) - \mathbf{s}_{\theta, \sigma}(\mathbf{x}_\sigma)\|_2^2 \\ &= \frac{\partial}{\partial \theta} \mathbb{E}_{\substack{\epsilon \sim \mathcal{N}(0, \mathbf{I}), \\ \mathbf{z} \sim p_{\mathbf{z}}}} \|\mathbf{s}_q(g_\theta(\mathbf{z}) + \sigma\epsilon) - \mathbf{s}_{\theta, \sigma}(g_\theta(\mathbf{z}) + \sigma\epsilon)\|_2^2 \\ &= \mathbb{E}_{\substack{\epsilon \sim \mathcal{N}(0, \mathbf{I}), \\ \mathbf{z} \sim p_{\mathbf{z}}}} \left\{ \frac{\partial}{\partial \theta} \left\{ \|\mathbf{s}_q(g_\theta(\mathbf{z}) + \sigma\epsilon) - \mathbf{s}_{\theta, \sigma}(g_\theta(\mathbf{z}) + \sigma\epsilon)\|_2^2 \right\} \frac{\partial g_\theta(\mathbf{z}) + \sigma\epsilon}{\partial \theta} \right. \end{aligned} \quad (10)$$

$$\left. - 2[\mathbf{s}_q(\mathbf{x}_\sigma) - \mathbf{s}_{\theta, \sigma}(\mathbf{x}_\sigma)]^T \frac{\partial}{\partial \theta} \mathbf{s}_{\theta, \sigma}(\mathbf{x}_\sigma) \Big|_{\mathbf{x}_\sigma = g_\theta(\mathbf{z}) + \sigma\epsilon} \right\} \quad (11)$$

$$\begin{aligned} &= \mathbb{E}_{\mathbf{x}_\sigma \sim p_{\sigma, \theta}} \left\{ \frac{\partial}{\partial \theta} \left\{ \|\mathbf{s}_q(\mathbf{x}_\sigma) - \mathbf{s}_{\theta, \sigma}(\mathbf{x}_\sigma)\|_2^2 \right\} \frac{\partial(\theta)}{\partial \theta} - 2[\mathbf{s}_q(\mathbf{x}_\sigma) - \mathbf{s}_{\theta, \sigma}(\mathbf{x}_\sigma)]^T \frac{\partial}{\partial \theta} \mathbf{s}_{\theta, \sigma}(\mathbf{x}_\sigma) \right\} \\ &= \text{Grad}_1(\theta) + \text{Grad}_1(\theta). \end{aligned} \quad (12)$$

□

B.2 Proof of Theorem 1

Proof. First, we prove a Lemma 2. This lemma has been used for proving the equivalence of Denoising Score Matching (Vincent, 2011; Zhou et al., 2024) and Standard Score Matching (Hyvärinen and Dayan, 2005) as we introduced in Section 3.

Lemma 2. *Let $\mathbf{u}(\cdot)$ be a vector-valued function, using the notations of Theorem 1. Let $q_\sigma(\mathbf{x}_\sigma | \mathbf{x}_0) = \mathcal{N}(\mathbf{x}_\sigma; \mathbf{x}_0, \sigma^2 \mathcal{I})$, then under mild conditions, the identity holds:*

$$\mathbb{E}_{\substack{\mathbf{x}_0 \sim p_{0, \theta}, \\ \mathbf{x}_\sigma | \mathbf{x}_0 \sim q_\sigma(\mathbf{x}_\sigma | \mathbf{x}_0)}} \mathbf{u}(\mathbf{x}_\sigma, \theta)^T \left\{ \mathbf{s}_{\theta, \sigma}(\mathbf{x}_\sigma) - \nabla_{\mathbf{x}_\sigma} \log q_\sigma(\mathbf{x}_\sigma | \mathbf{x}_0) \right\} = 0, \quad \forall \theta. \quad (13)$$

Proof of Lemma 2. Recall the definition of $p_{\sigma, \theta}$ and $\mathbf{s}_{\theta, \sigma}$:

$$p_{\sigma, \theta}(\mathbf{x}_\sigma) = \int q_\sigma(\mathbf{x}_\sigma | \mathbf{x}_0) p_{\theta, 0}(\mathbf{x}_0) d\mathbf{x}_0 \quad (14)$$

$$\mathbf{s}_{\theta, \sigma}(\mathbf{x}_\sigma) = \int \nabla_{\mathbf{x}_\sigma} \log q_\sigma(\mathbf{x}_\sigma | \mathbf{x}_0) \frac{q_\sigma(\mathbf{x}_\sigma | \mathbf{x}_0) p_{\theta, 0}(\mathbf{x}_0)}{p_{\sigma, \theta}(\mathbf{x}_\sigma)} d\mathbf{x}_0. \quad (15)$$

We may use \mathbf{u} for short of $\mathbf{u}(\mathbf{x}_\sigma, \theta)$. We have

$$\mathbb{E}_{\mathbf{x}_\sigma \sim p_{\sigma, \theta}} \mathbf{u}^T \mathbf{s}_{\theta, \sigma}(\mathbf{x}_\sigma) = \mathbb{E}_{\mathbf{x}_\sigma \sim p_{\sigma, \theta}} \mathbf{u}^T \int \nabla_{\mathbf{x}_\sigma} \log q_\sigma(\mathbf{x}_\sigma | \mathbf{x}_0) \frac{q_\sigma(\mathbf{x}_\sigma | \mathbf{x}_0) p_{\theta, 0}(\mathbf{x}_0)}{p_{\sigma, \theta}(\mathbf{x}_\sigma)} d\mathbf{x}_0 \quad (16)$$

$$= \int p_{\sigma, \theta}(\mathbf{x}_\sigma) \mathbf{u}^T \int \nabla_{\mathbf{x}_\sigma} \log q_\sigma(\mathbf{x}_\sigma | \mathbf{x}_0) \frac{q_\sigma(\mathbf{x}_\sigma | \mathbf{x}_0) p_{\theta, 0}(\mathbf{x}_0)}{p_{\sigma, \theta}(\mathbf{x}_\sigma)} d\mathbf{x}_0 d\mathbf{x}_\sigma \quad (17)$$

$$= \int \int \mathbf{u}^T \nabla_{\mathbf{x}_\sigma} \log q_\sigma(\mathbf{x}_\sigma | \mathbf{x}_0) q_\sigma(\mathbf{x}_\sigma | \mathbf{x}_0) p_{\theta, 0}(\mathbf{x}_0) d\mathbf{x}_0 d\mathbf{x}_\sigma \quad (18)$$

$$= \mathbb{E}_{\substack{\mathbf{x}_0 \sim p_{0, \theta}, \\ \mathbf{x}_\sigma | \mathbf{x}_0 \sim q_\sigma(\mathbf{x}_\sigma | \mathbf{x}_0)}} \mathbf{u}^T \nabla_{\mathbf{x}_\sigma} \log q_\sigma(\mathbf{x}_\sigma | \mathbf{x}_0) \quad (19)$$

□

Next, we turn to prove the Theorem 1. Taking θ gradient on both sides of identity equation 13, we have

$$\begin{aligned} & \mathbb{E}_{\mathbf{x}_\sigma \sim p_{\theta, \sigma}} \left\{ \frac{\partial}{\partial \theta} \mathbf{u}(\mathbf{x}_\sigma, \theta)^T \mathbf{s}_{\sigma, \theta}(\mathbf{x}_\sigma) + \mathbf{u}(\mathbf{x}_\sigma, \theta)^T \frac{\partial}{\partial \theta} \mathbf{s}_{\sigma, \theta}(\mathbf{x}_\sigma) \right\} + \mathbb{E}_{\mathbf{x}_\sigma \sim p_{\theta, \sigma}} \frac{\partial}{\partial \mathbf{x}_\sigma} \left\{ \mathbf{u}(\mathbf{x}_\sigma, \theta)^T \mathbf{s}_{\sigma, \theta}(\mathbf{x}_\sigma) \right\} \frac{\partial \mathbf{x}_\sigma}{\partial \theta} \quad (20) \\ &= \mathbb{E}_{\substack{\mathbf{x}_0 \sim p_{0, \theta}, \\ \mathbf{x}_\sigma | \mathbf{x}_0 \sim q_\sigma(\mathbf{x}_\sigma | \mathbf{x}_0)}}} \frac{\partial}{\partial \theta} \mathbf{u}(\mathbf{x}_\sigma, \theta)^T \nabla_{\mathbf{x}_\sigma} \log q_\sigma(\mathbf{x}_\sigma | \mathbf{x}_0) + \mathbb{E}_{\substack{\mathbf{x}_0 \sim p_{0, \theta}, \\ \mathbf{x}_\sigma | \mathbf{x}_0 \sim q_\sigma(\mathbf{x}_\sigma | \mathbf{x}_0)}}} \left\{ \frac{\partial}{\partial \mathbf{x}_\sigma} \left[\mathbf{u}(\mathbf{x}_\sigma, \theta)^T \nabla_{\mathbf{x}_\sigma} \log q_\sigma(\mathbf{x}_\sigma | \mathbf{x}_0) \right] \frac{\partial \mathbf{x}_\sigma}{\partial \theta} \right. \\ & \left. + \mathbf{u}(\mathbf{x}_\sigma, \theta)^T \frac{\partial}{\partial \mathbf{x}_0} \nabla_{\mathbf{x}_\sigma} \log q_\sigma(\mathbf{x}_\sigma | \mathbf{x}_0) \frac{\partial \mathbf{x}_0}{\partial \theta} \right\} \end{aligned}$$

Notice that one can have

$$\mathbb{E}_{\mathbf{x}_\sigma \sim p_{\theta, \sigma}} \left\{ \frac{\partial}{\partial \theta} \mathbf{u}(\mathbf{x}_\sigma, \theta)^T \right\} \mathbf{s}_{\sigma, \theta}(\mathbf{x}_\sigma) = \mathbb{E}_{\substack{\mathbf{x}_0 \sim p_{0, \theta}, \\ \mathbf{x}_\sigma | \mathbf{x}_0 \sim q_\sigma(\mathbf{x}_\sigma | \mathbf{x}_0)}}} \frac{\partial}{\partial \theta} \mathbf{u}(\mathbf{x}_\sigma, \theta)^T \nabla_{\mathbf{x}_\sigma} \log q_\sigma(\mathbf{x}_\sigma | \mathbf{x}_0)$$

by substituting $\mathbf{u}(\mathbf{x}_\sigma, \theta)$ with $\frac{\partial}{\partial \theta} \mathbf{u}(\mathbf{x}_\sigma, \theta)$ in equation (13).

This allows us to cancel out the corresponding terms from equation (20), and we have

$$\begin{aligned} & \mathbb{E}_{\mathbf{x}_\sigma \sim p_{\theta, \sigma}} \left\{ \mathbf{u}(\mathbf{x}_\sigma, \theta)^T \frac{\partial}{\partial \theta} \mathbf{s}_{\sigma, \theta}(\mathbf{x}_\sigma) \right\} + \mathbb{E}_{\mathbf{x}_\sigma \sim p_{\theta, \sigma}} \frac{\partial}{\partial \mathbf{x}_\sigma} \left\{ \mathbf{u}(\mathbf{x}_\sigma, \theta)^T \mathbf{s}_{\sigma, \theta}(\mathbf{x}_\sigma) \right\} \frac{\partial \mathbf{x}_\sigma}{\partial \theta} \quad (21) \\ &= \mathbb{E}_{\substack{\mathbf{x}_0 \sim p_{0, \theta}, \\ \mathbf{x}_\sigma | \mathbf{x}_0 \sim q_\sigma(\mathbf{x}_\sigma | \mathbf{x}_0)}}} \left\{ \frac{\partial}{\partial \mathbf{x}_\sigma} \left[\mathbf{u}(\mathbf{x}_\sigma, \theta)^T \nabla_{\mathbf{x}_\sigma} \log q_\sigma(\mathbf{x}_\sigma | \mathbf{x}_0) \right] \frac{\partial \mathbf{x}_\sigma}{\partial \theta} + \mathbf{u}(\mathbf{x}_\sigma, \theta)^T \frac{\partial}{\partial \mathbf{x}_0} \nabla_{\mathbf{x}_\sigma} \log q_\sigma(\mathbf{x}_\sigma | \mathbf{x}_0) \frac{\partial \mathbf{x}_0}{\partial \theta} \right\} \end{aligned}$$

This gives rise to

$$\begin{aligned} & \mathbb{E}_{\mathbf{x}_\sigma \sim p_{\theta, \sigma}} \left\{ \mathbf{u}(\mathbf{x}_\sigma, \theta)^T \frac{\partial}{\partial \theta} \mathbf{s}_{\sigma, \theta}(\mathbf{x}_\sigma) \right\} \quad (22) \\ &= \mathbb{E}_{\substack{\mathbf{x}_0 \sim p_{0, \theta}, \\ \mathbf{x}_\sigma | \mathbf{x}_0 \sim q_\sigma(\mathbf{x}_\sigma | \mathbf{x}_0)}}} \left\{ \frac{\partial}{\partial \mathbf{x}_\sigma} \left[\mathbf{u}(\mathbf{x}_\sigma, \theta)^T \{ \nabla_{\mathbf{x}_\sigma} \log q_\sigma(\mathbf{x}_\sigma | \mathbf{x}_0) - \mathbf{s}_{\theta, \sigma}(\mathbf{x}_\sigma) \} \right] \frac{\partial \mathbf{x}_\sigma}{\partial \theta} + \mathbf{u}(\mathbf{x}_\sigma, \theta)^T \frac{\partial \nabla_{\mathbf{x}_\sigma} \log q_\sigma(\mathbf{x}_\sigma | \mathbf{x}_0)}{\partial \mathbf{x}_0} \frac{\partial \mathbf{x}_0}{\partial \theta} \right\} \end{aligned}$$

We now define the following loss function

$$\mathcal{L}_2(\theta) = \mathbb{E}_{\substack{\mathbf{x}_0 \sim p_{0, \theta}, \\ \mathbf{x}_\sigma | \mathbf{x}_0 \sim q_\sigma(\mathbf{x}_\sigma | \mathbf{x}_0)}}} \left\{ \mathbf{u}(\mathbf{x}_\sigma, \text{sg}[\theta])^T \{ \nabla_{\mathbf{x}_\sigma} \log q_\sigma(\mathbf{x}_\sigma | \mathbf{x}_0) - \mathbf{s}_{\text{sg}[\theta], \sigma}(\mathbf{x}_\sigma) \} \right\} \quad (23)$$

with $\mathbf{u}(\mathbf{x}_\sigma, \theta) = -2\{ \nabla_{\mathbf{x}_\sigma} \log q_\sigma(\mathbf{x}_\sigma) - \mathbf{s}_{\sigma, \theta}(\mathbf{x}_\sigma) \}$. Its gradient becomes

$$\begin{aligned} & \mathbb{E}_{\mathbf{x}_\sigma \sim p_{\theta, \sigma}} \left\{ -2\{ \nabla_{\mathbf{x}_\sigma} \log q_\sigma(\mathbf{x}_\sigma) - \mathbf{s}_{\sigma, \theta}(\mathbf{x}_\sigma) \}^T \frac{\partial}{\partial \theta} \mathbf{s}_{\sigma, \theta}(\mathbf{x}_\sigma) \right\} \\ &= \frac{\partial}{\partial \theta} \mathbb{E}_{\substack{\mathbf{x}_0 \sim p_{0, \theta}, \\ \mathbf{x}_\sigma | \mathbf{x}_0 \sim q_\sigma(\mathbf{x}_\sigma | \mathbf{x}_0)}}} \left\{ \mathbf{u}(\mathbf{x}_\sigma, \text{sg}[\theta])^T \{ \nabla_{\mathbf{x}_\sigma} \log q_\sigma(\mathbf{x}_\sigma | \mathbf{x}_0) - \mathbf{s}_{\text{sg}[\theta]}(\mathbf{x}_\sigma, t) \} \right\} \quad (24) \end{aligned}$$

by applying the above result in (22). \square

C Experiments

C.1 Experiment Details on 2D Synthetic Sampling

Model architectures. In our 2D synthetic data experiments, a 4-layer Multi-Layer Perceptron (MLP) neural network, equipped with 200 neurons in each layer, serves as our sampler. This network employs a LeakyReLU activation function with a leakage parameter of 0.2. Concurrently, the score network is also an MLP with 4 layers and 200 neurons per layer, utilizing GELU activation.

Comparison of DFT and KL training methods. In this work, we propose the DFT training method for neural implicit samplers, which is built on minimizing the Fisher divergence between slightly perturbed neural sampler distribution and the un-normalized target distribution. The DFT has similarities to previous methods such as KL training (Luo et al., 2024), which also has a paradigm of alternative training an online score network, and neural implicit samplers. However, DFT is different from KL training. In 2D target distribution sampling and the Bayesian logistic regression experiment, we empirically find that DFT training shows better performances than KL training. The reason behind such a plausible performance of the DFT sampler might be the different divergence that DFT and KL samplers are using. Besides, the small perturbation to sampler distributions also facilitates the distribution density of the DFT sampler to spread in all space, which potentially stabilizes the training dynamics.

C.2 Experiment Details on Bayesian Regression

Experiment settings. Following the setup in Hu et al. (2018), we define the prior of the weights as $p(w | \alpha) = \mathcal{N}(w; 0, \alpha^{-1})$ and $p(\alpha) = \text{Gamma}(\alpha; 1, 0.01)$. The Covertypes dataset Blackard and Dean (1999), comprising 581,012 samples with 54 features, is split into a training set (80%) and a testing set (20%). Our methods are benchmarked against Stein GAN, SVGD, SGLD, DSVI Titsias and Lázaro-Gredilla (2014), KSD-NS, and Fisher-NS Hu et al. (2018). While SGLD, DSVI, and SVGD are trained for 3 epochs (approximately 15k iterations), neural network-based methods (Fisher-NS, KSD-NS, Stein GAN, KL-NS, and DFT-NS) are trained until convergence. Given the equivalence of Fisher-NS Hu et al. (2018), we train the implicit sampler using the denoising Fisher training method. The learning rate for both the score network and the sampler is set to 0.0002. The target distribution is approximated using 500 random data samples, with the score estimation phase set to 2. The logistic regression model’s test accuracy is evaluated using 100 samples from the trained sampler.

For Bayesian inference, we adopt the same configuration as in Hu et al. (2018). The neural samplers are constructed with a 4-layer MLP containing 1024 hidden units per layer and GELU activations. The sampler’s output dimension is 55, with an input dimension of 550, aligning with the setup in Hu et al. (2018). The score network mirrors the sampler’s architecture but with an input dimension of 55. Adam optimizers with a learning rate of 0.0002 and default beta values are used for both networks. A batch size of 100 is employed for training the sampler, with the score network updated twice for every sampler update. Standard score matching is used to train the score network. The sampler undergoes 10k iterations per repetition, with 30 independent repetitions to determine the mean and standard deviation of the test accuracy. For SGLD, the learning rate follows $0.1/(t+1)^{0.55}$ as recommended in Welling and Teh (2011), with the last 100 points averaged for evaluation. DSVI uses a learning rate of $1e-07$ with 100 iterations per stage. SVGD employs an RBF kernel with bandwidth determined by the median trick Liu and Wang (2016), utilizing 100 particles with a step size of 0.05 for evaluation.

Model architectures. Our model employs 4-layer MLP neural networks for both the sampler and the score network. The GELU Hendrycks and Gimpel (2016) activation function is utilized for both, with a hidden dimension of 1024. The sampler’s input dimension is set to 128.

C.3 Experiment Details on Sampling from EBMs

Datasets and model architectures. We pre-train a deep (multi-scale) Energy-Based Model (EBM) Li et al. (2019), denoted as $E_d(\cdot)$, with 12 residual layers He et al. (2015), following the approach in DeepEBM (Li et al., 2019). The noise levels are initialized at $\sigma_{min} = 0.3$ and capped at $\sigma_{max} = 3.0$. The energy for varying noise levels is modeled as $E_\sigma(\mathbf{x}) = f(\mathbf{x})/\sigma$. With a learning rate of 0.001, the EBM is pre-trained for 200k iterations. Samples are extracted from the deep EBM using an annealed Langevin dynamics algorithm similar to that in Li et al. (2019). Our implicit sampler is a neural network comprising four inverse convolutional layers with hidden dimensions of 1024, 512, 256, and 3. Each layer incorporates 2D BatchNormalization and a LeakyReLU activation with a leak parameter of 0.2. The implicit generator’s prior is a standard Multivariate Gaussian distribution. The score network adheres to a UNet architecture adapted from the repository³. To align with the multi-scale EBM design, the score function is parameterized as $S_\sigma(\mathbf{x}) := S(\mathbf{x})/\sigma$.

Training details. The deep EBM is pre-trained on the MNIST dataset. The pre-trained EBM is then treated as a multi-scale un-normalized target distribution. We employ the DFT training method to refine the score

³https://github.com/huggingface/notebooks/blob/main/examples/annotated_diffusion.ipynb

network and generator, aiming to align the generator with the target distribution. Both the generator and score network are initialized randomly. During each training iteration, a noise level σ is randomly selected within the range $[\sigma_{min}, \sigma_{max}]$. A sample is generated and Gaussian noise with variance σ^2 is added. The score network is then updated using denoising score matching on the generated samples. Subsequently, a batch of samples with the same variance of Gaussian noise is generated, and the generator’s parameters are updated using the gradient estimation from Algorithm 1. The Adam optimizer with a learning rate of 0.0001 is used for both networks. For the score network, the optimizer parameters are set to $\beta_0 = 0.9$ and $\beta_1 = 0.99$. For the generator, these are set to $\beta_0 = 0$ and $\beta_1 = 0.99$.

Evaluation metrics. The Frechet Inception Distance (FID) [Heusel et al. \(2017\)](#) is adapted to qualitatively assess the generated samples’ quality. An MNIST image classifier with a WideResNet [Zagoruyko and Komodakis \(2016\)](#) architecture, having a depth of 16 and a widening factor of 8, is pre-trained. The Wasserstein distance in the feature space of this classifier is calculated using the FID method.